Numerical and experimental investigation of the flow field around a surface piercing plate

*G. Colicchio** *U.P. Bulgarelli** *J.R. Chaplin***
g.colicchio@insean.it up.bulgarelli@insean.it j.r.chaplin@soton.ac.uk
∗ INSEAN, The Italian Ship Model Basin, Roma – Italy, ∗∗ University of Southampton, Southampton – UK.

A large variety of fluid dynamic problems is characterized by strong deformations of the air-water interface. A body moving in water or standing in a current can lead to the breaking of the free surface, air entrainment and generation of vorticity. The study of all these aspects for a generic 3D body can be extremely difficult, particularly because the different phenomena involved interact with each other. With the aim of understanding the physical mechanisms present, both numerical and experimental analyses have been performed for the canonical case of a 2D flat plate moving in initially calm water. This simple problem not only provides a way of studying the fundamental elements described above, but also constitutes a valid benchmark for the validation of the numerical codes dealing with strong deformations of free surfaces and wave-body interactions.

1 Description of the problem

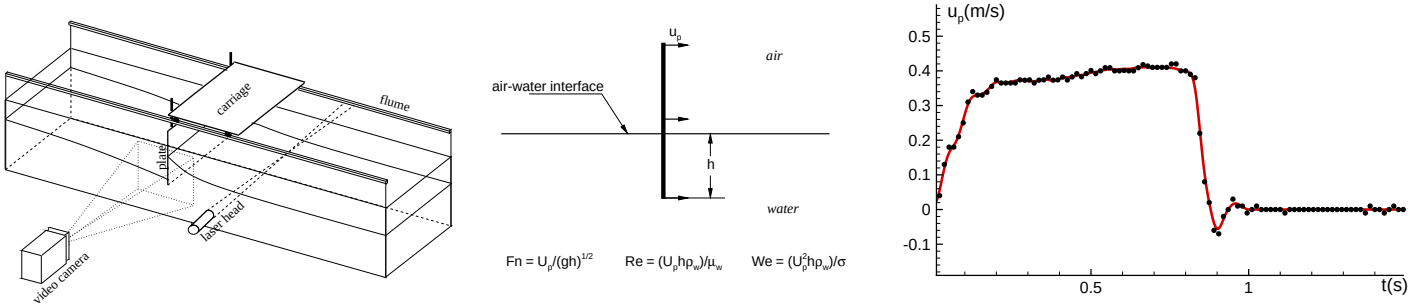

Figure 1: Left and center: sketch of the experimental set up and parameters of the problem. Right: time history of the velocity u_p of the vertical plate.

The problem analyzed here is briefly described in the sketches of figure 1. A vertical plate, partially immersed in the water initially at rest, starts to move from left to right with the velocity shown in figure 1. The evolution of the flow field around the plate has been studied both numerically and experimentally.

The experimental apparatus The experiments were performed in a flume 0.420mm wide, 18m long and at a water depth of 0.6m. An aluminium plate was towed along the flume and the flow features are captured by a video-camera placed at the side of the flume, to visualize the air-water interface displacement, and a 2 components Argon-Ion Laser Doppler anemometer (LDA) to measure the velocity field.

The vertical plate is 300mm long, 415mm large and 5mm wide. A soft plastic material was used at the two sides of the plate, thus allowing an almost perfect contact with the walls of the flume; leaks at the two sides of the plate were reduced to a minimum to ensure two-dimensional flow conditions during the tests.

Different devices were used to control the flow conditions and to measure the relevant physical quantities. An optical encoder mounted on a drive shaft measured the velocity of the plate with a sample rate of 200Hz. A PC controlled the motion of a DC motor connected through a ballscrew to the carriage. The calibration of the images for the measurements was done using a grid printed on the glass wall of the flume. For a better definition of the air-water interface a fluorescent dye was dispersed in the water and illuminated by two halogen lamps.

The numerical solver A multi-phase fluid method has been adopted to model the behaviour of air and water, both considered incompressible. The flow field is described through the solution of the Navier-Stokes (NS) equations with an approximate projection method. The interface separating the two phases is captured by a *level-set* function. A second order approximation is used both in the spatial and time discretization, the latter is obtained through a predictor-corrector scheme, where the projection step is performed at each sub-step of the time integration scheme.

A variable coefficients ENO scheme and a redefined reinitalization procedure for the level set function have been used respectively for higher accuracy in the discretization of the advective term and of the interface. An exponential smoothing of the density and the split of the Poisson equations for the pressure terms improved the stability properties of the two-phase Navier-Stokes solver. For details of the NS solver refer to Colicchio (2004).

2 Description of the flow field

For this set of experiments the maximum velocity of the plate was 0.5m/s and the initial submergence $h = 0.18$m. These conditions lead to Froude number $Fn = 0.37$, a Reynolds number $Re = 5.9 \cdot 10^4$ and Weber number $We = 388$.

Figure 2 presents a series of experimental pictures referring to the deformation of the free surface, when the plate moves as shown in figure 1.

The white lines in the snapshots represent the numerical results (a stretched mesh has been used to discretize the flow, close to the plate the mesh is uniform with $\Delta x = \Delta y = h/45$ and $\Delta t = 8 \cdot 10^{-4}$s) and they are superimposed on the black and white experimental pictures. The overall evolution of the free surface is well captured by the NS solver.

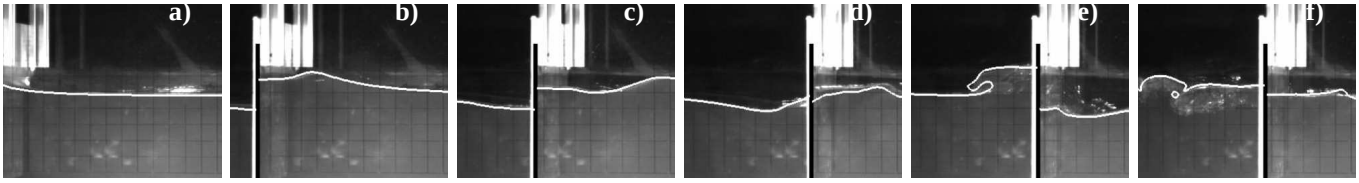

Figure 2: Deformation of the free surface: comparison between numerical and experimental results. In each plot, the black and white background is the experimental video-image of the free surface deformation on one of the glass sides of the tank, the white line the numerical free surface. The snapshots refer to the times a) t=0.128s, b) t=0.384s, c) t=0.640s, d) t=0.896s, e) t=1.152s and f) t=1.408s. The grid on the experimental pictures presents a mesh size of 3cm both in the x and y directions.

When the plate starts to move the free surface on the front side deforms more than on the back. On the right side (see figure 2), the plate behaves as a wavemaker and causes the formation of a wave that moves from left to right. The development of this wave can be observed from figure 2-a to 2-c. On the back of the plate the body motion causes a depression that sucks down the air-water interface.

When the plate stops (see figure 2-d) some differences between numerical and experimental results appear. The numerical free surface in the front region is quite different from the physical one, while no difference can be noted at the back of the plate. Figure 2-d refers to t=0.896s when the plate is stopping and u_p is reaching its lowest negative value. It is to be noted that from t=0.87s to t=1.2s the experimental plate rotates slightly around the upper hinge of the carriage. Apart from the small differences between numerical and experimental velocities, these oscillations can be the cause of the disagreement between the two sets of data. The differences decrease as the time goes on.

At the time at which the plate stops, a large deformation of the interface occurs at the back of the plate. The inertia of the water causes its rise and, later, the liquid fall under gravity, forming a plunging breaker (see figure 2-e). The plunging jet re-enters the water in figure 2-f. The agreement between numerical and experimental results is good both in the formation of the plunging jet and in its breaking. Moreover the numerical and experimental data show a similar behaviour of the splash up. The water first rises and then falls, forming two jets one on the left and one on the right (see figure 2-f).

3 Evolution of the vorticity in the flow field

The good agreement between numerical and experimental data in figure 2 allows the use of the NS solver and of the experiments as two complementary tools to investigate the evolution of the flow field around the plate. Here, the attention is focused on the generation of vorticity in two regions: in the back where the plunging jet impacts onto the free surface (see figure 2-f) and at the lower tip of the plate.

Vorticity after the breaking When a plunging jet hits the air-water interface, a strong vorticity is generated at the contact region. Here, in particular, two counter-rotating vortices are generated after the backward breaking. They form a vortex pair moving downward and toward the plate. The two vortices are characterized respectively by a clockwise rotation on the left and an anticlockwise rotation on the right. Therefore their mutual action induces a downward motion. As the right vortex is more intense than the left one, the pair moves also to the right.

Figure 2-f highlights the region of high vorticity by the presence of a bubbly regions. In fact, the vortex cores are characterized by low dynamic pressure. Figure 3 shows the relation between bubble concentration and vorticity by the superposition of the numerical vorticity and pressure onto the experimental images. In the upper part of the vortices, this causes pressure gradients opposite to the hydrostatic pressure gradients, trapping any bubbles that occur in this region (see Petitjeans, 2003). Therefore, when the vortex cores move downward, the low pressure areas associated with them bring the bubbles down as well. The lower boundary of the bubbly region (in figure 3 the bubbles appear as dark dots in water) corresponds roughly to the most curved pressure contours.

While moving downward, the vorticity is diffused by viscosity, consequently the regions of low dynamic pressure decrease in size and intensity. So that the buoyancy results comparable with the suction force induced by the vortex core and a larger number of bubbles leaves the high vorticity region as a kind of wake behind the vortex centers.

LDA measurements were not performed in this region. However, it is sensible to think that the presence of bubbles would have produced rather scattered values of velocity.

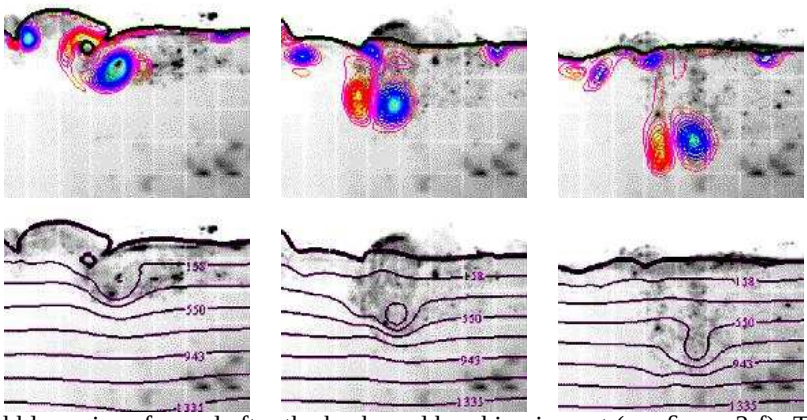

Figure 3: Vorticity and bubbly regions formed after the backward breaking impact (see figure 3-f). The bubbles concentrate in the vortical zone. Top: vorticity contours superimposed on the experimental images. Bottom: pressure contours superimposed on the video images. The figures refer to the left side of the plate at the times t=1.408s, 1.536s and 1.664s, form left to right.

Vorticity at the lower tip of the plate A corner is a continuous source of vorticity in a current. Here, the evolution of the vorticity generated at the lower tip of the plate is analyzed. Figure 4 shows the evolution of the vorticity in the flow field. A first counter-clockwise vortex is shed at the lower tip by the rightward motion of the plate. The numerical vortex sheet is not severely influenced by the deformation of the free surface, in fact it seems stable by the calculation. When the plate stops, a second clockwise vorticity is generated. This one is unstable instead, in fact the vortex sheet rolls up onto itself.

The LDA measurements have been used to confirm the numerical results. The experimental measurements are collected at discrete points displaced onto four vertical columns and nine rows but only a 3×3 table is analyzed here. The reported points of measurement are spaced by 0.08m in the vertical direction and by 0.02m and 0.04m in the horizontal direction. The highest point is located 0.026m below the free surface and the most left point is 0.2185m distant from the initial position of the plate. Each location is labeled with a capital letter indicating the column and a number referring to the row (see figure 4 for the relative position of the measurement locations).

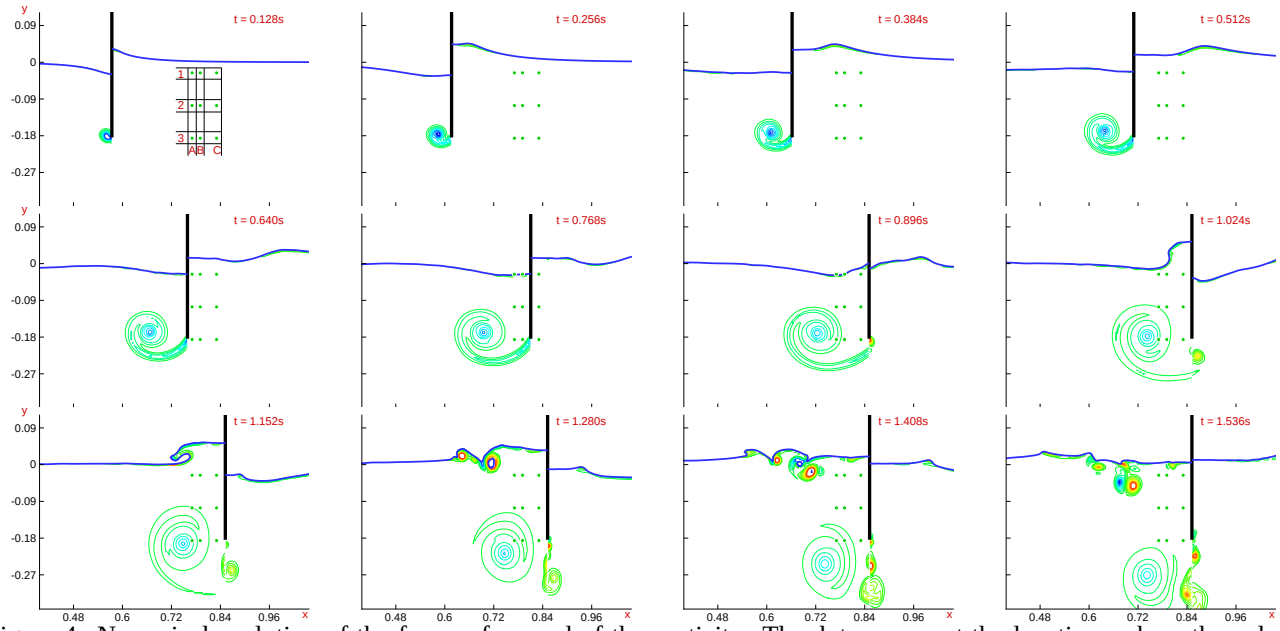

Figure 4: Numerical evolution of the free surface and of the vorticity. The dots represent the locations where the velocity is measured experimentally. The still water depth was 0.7m.

The numerical and experimental velocities in those points are shown in figures 5. The two sets of data agree quite well, with larger discrepancies between the different data when the plate stops ($t \simeq 0.9$s).

All the columns present similar behaviours. For example, because the water in the uppermost row is diverted upward by the plate motion, there is the creation of a first wave on the right side of the plate (see figure 4). When the first wave detaches from the plate on the right and goes over the measurement points, the points A1, B1 and C1 present a local maximum in the horizontal component of the velocity, u, and an almost simultaneously zero value of the vertical one, v.

As the wave passes the measurement points, v assumes negative values. In fact, the measurement points enter the region of influence of the lower tip of the plate. There, most of the fluid is diverted below the plate. The closer the point is to the lower tip, the higher this effect is and, consequently, the larger the negative value assumed by v becomes. Because of this behaviour, before the plate crosses the test section, the minimum value reached by v decreases from row 1 to row 3

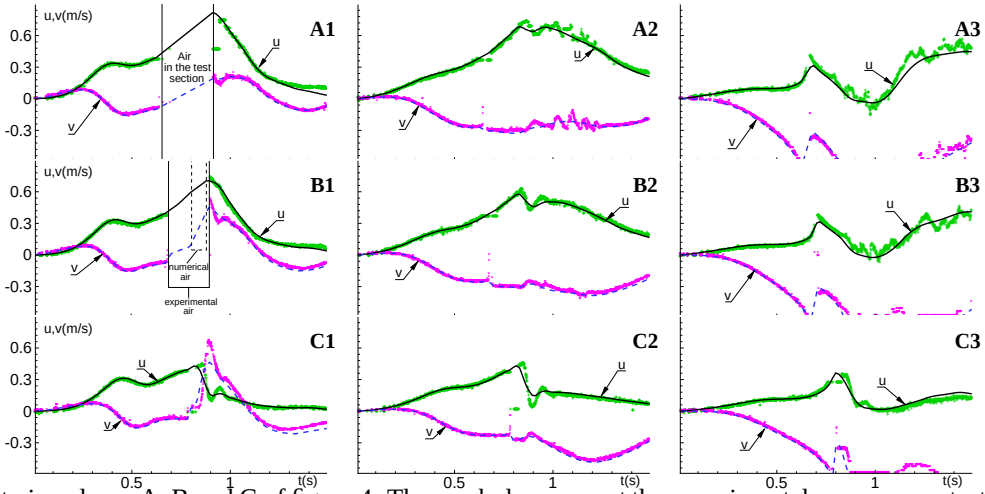

Figure 5: Velocity in column A, B and C of figure 4. The symbols represent the experimental measurements, the solid black lines and the dashed blue lines represent respectively the numerical u and v components of the velocity.

When the plate crosses the test section, the experimental velocity shows a constant value of u. This is equal to the instantaneous velocity of the plate. The persisting constant value is the result of an error in the measurements generated by the reflections of the laser beam on the plate.

At the same time, a small jump appears in the vertical velocity, due to the passage of the measurement point from one side of the plate to the other. This jump is not large at rows 1 and 2. Because no major deformation of the free surface alters significantly the flow field at either side of the plate. The passage of measurement locations from the right side of the plate to the left causes two gaps in the data of points A1 and B1. The gap is common both to the numerical and to the experimental results and it is due to a local water level lower than $y = -0.023m$.

Row 3 is below the lower tip of the plate. And the related velocity jump is due to the passage of the vortex sheet, characterized by a rapid change of velocity across it (Saffman 1992).

Later on, the upper rows 1-2 present an increase of the horizontal velocity. They are in the upper and right part of the vortex released at the lower tip of the plate (see figure 4); this means that a positive velocity contribution due to the vortex is added to the velocity of translation of the plate. Row 3 presents a cusp in the horizontal velocity due to the vortex sheet; this is captured by the numerics although the numerical results appear more smoothed than the experimental velocity.

When the plate stops almost abruptly at t=0.9s, both the vertical and the horizontal components of the velocity show a jump. This jump is present in each column but it is more marked in column C that is the closest to the plate at that time.

After the stop, the points on column A are crossed by the vortex sheet. When this occurs, some oscillations appear in the measured velocities. The link between the passage of the vortex sheet and the oscillations can be deduced cross checking figures 4 and 5. The oscillations appear at the same time as the contours of strong vorticity arrive at the measurement points, and they are not present in column C that is not affected by vorticity (see figure 4). However, they are not present in the numerical data, and the reason for their absence is not clear. Considering that no bubble is present in the flow (at least within the resolution of the video camera), and that the frequency of the oscillation is low enough to exclude effects of turbulence, three possible explanations can be given. First, the vortex sheet is unstable, generating side vortices velocity oscillations. Koumoutsakos & Shiels (1996) show that a plate accelerating in an incompressible fluid can create an unstable vortex sheet. The velocity of the plate analyzed here is subject to a phase of acceleration, potentially responsible for the instabilities in the vortex sheet. If this is the case, it is likely that the numerical calculations do not capture the oscillations because the mesh is not sufficiently refined around the lower tip of the plate. A second explanation comes from the comparison between the numerical and the experimental velocity jumps at point A9. The measured vertical velocity jump across the vortex sheet is captured well numerically in figure 5-A9, but the corresponding cusp in the horizontal component is smoothed by the numerics. If a similar smoothing occurred in smaller jumps, the numerics would not reproduce the oscillations in the horizontal velocity. The rotation of the plate around the upper hinge is a further possible explanation. The amplitude of this oscillation is large enough to cause the displacement of the vortex sheet and consequently to cause the abrupt changes in velocity. There is no means here to state with confidence which one of these possibilities is most likely, and they are probably combined in reality to give the results shown in figures 5.

The present research activity is developed in the framework of the "Programma Sicurezza" funded by *Ministero Infrastrutture e Trasporti*.

References

COLICCHIO, G. (2004). Violent disturbance and fragmentation of the free surface. *Ph.D Thesis, University of Southampton (UK)*.

KOUMOUTSAKOS, P. & D. SHIELS (1996). Simulation of the viscous fbw normal to an impulsively started and uniformly accelerated fbt plate. *J. Fluid Mech. 328*, 177–227.

PETITJEANS, P. (2003). Stretching of a vortical structure fi laments of vorticity. *Europhysics News 34*.

SAFFMAN, P. G. (1992). Vortex Dynamics. *Cambridge University Press*.